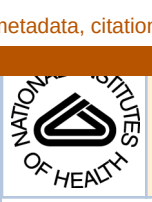

Published in final edited form as:
Mol Imaging. 2009 ; 8(4): 230–237.

Repetitive Noninvasive Monitoring of HSV1-tk-Expressing T Cells Intravenously Infused into Nonhuman Primates Using Positron Emission Tomography and Computed Tomography with ^{18}F-FEAU

Gianpietro Dotti[*], **Mei Tian**[*], **Barbara Savoldo**[*], **Amer Najjar**, **Laurence J.N. Cooper**, **James Jackson**, **Amanda Smith**, **Osama Mawlawi**, **Rajesh Uthamanthil**, **Agatha Borne**, **David Brammer**, **Vincenzo Paolillo**, **Mian Alauddin**, **Carlos Gonzalez**, **David Steiner**, **William K. Decker**, **Frank Marini**, **Steven Kornblau**, **Catherine M. Bollard**, **Elizabeth J. Shpall**, and **Juri G. Gelovani**

Departments of Experimental Diagnostic Imaging, Nuclear Medicine, Imaging Physics, Veterinary Medicine and Surgery, Stem Cell Transplantation and Cellular Therapy, and Pediatrics, The University of Texas M.D. Anderson Cancer Center, and the Center for Cell and Gene Therapy, Baylor College of Medicine, Houston, TX.

Abstract

Adoptive transfer of antigen-specific cytotoxic T lymphocytes (CTLs) has been successfully used to treat patients with different types of cancer. However, the long-term spatial-temporal dynamics of the distribution of systemically infused CTLs remains largely unknown. Noninvasive imaging of adoptively transferred CTLs using molecular-genetic reporter imaging with positron emission tomography and computed tomography (PET-CT) represents an innovative approach to understanding the long-term migratory patterns and therapeutic potential of adoptively transferred T cells. Here we report the application of repetitive PET-CT imaging with [^{18}F]fluoro-5-ethyl-1-beta-D-arabinofuranosyluracil (^{18}F-FEAU) in two nonhuman primates demonstrating that autologous polyclonal macaque T lymphocytes activated and transduced with a retroviral vector encoding for the sr39 mutant herpes simplex virus 1 thymidine kinase (*sr39HSV1-tk*) reporter gene can be detected after intravenous infusion in discrete lymphoid organs and in sites of inflammation. This study represents a proof of principle and supports the application of ^{18}F-FEAU PET-CT imaging for monitoring the distribution of intravenously administered *sr39HSV1-tk* gene–transduced CTLs in humans.

Adoptive Transfer of Antigen-Specific Cytotoxic T Lymphocytes (CTLs) has been successfully used to treat patients with melanoma,[1,2] Hodgkin lymphoma[3] and nasopharyngeal carcinoma.[4,5] Moreover, infusion of gene-modified T cells expressing chimeric antigen receptors (CARs) or transgenic α β T-cell receptor chains represents an innovative approach to expand the application of T-cell therapies to other hematologic malignancies and solid tumors.[6,7]

Surrogate measurements of an effect of CTL infusion remain a crucial component of these studies. Compelling results have been obtained regarding sustained T-cell persistence and

Address reprint requests to: Juri G. Gelovani, Md, PhD, Department of Experimental Diagnostic Imaging, The University of Texas M.D. Anderson Cancer Center, 1515 Holcombe Boulevard, Houston, TX 77030; jgelovani@mdanderson.org.
[*]Authors who contributed equally to this work.

Financial disclosure of reviewers: None reported.

trafficking using “gene marking” in which adoptively transferred CTLs were serially detected by polymerase chain reaction (PCR) amplification in the peripheral blood and tumor biopsies of treated patients.[3,8,9] In recent studies, PCR amplification was also used to detect the persistence and localization of CAR-modified T lymphocytes.[6,10] In addition to describing the presence of T cells, the functional status of infused T cells has been demonstrated by interferon-γ ELISPOT assay and major histocompatibility complex multimers used to quantify the frequency of CTL precursors.[1–3,11]

A limitation of repetitive measurements of T-cell number and function based on longitudinal sampling of blood and tumor is that it does not allow assessment of the dynamic and spatial-temporal distribution of adoptively transferred CTLs. This limitation can be overcome by the application of noninvasive, accurate, and sensitive whole-body imaging technologies allowing repetitive measurement in vivo of these cells. This could be achieved by repetitive positron emission tomography and computed tomography (PET-CT) imaging with 2′-fluoro-2′-deoxy-1-β-D-arabinofuranosyl-5-iodouracil (FIAU), 9-(4-[^{18}F]fluoro-3-(hydroxymethyl) butyl)guanine (^{18}F-FHBG), or 2′-[^{18}F]fluoro-5-ethyl-1-beta-D-arabinofuranosyluracil (^{18}F-FEAU) of T cells genetically labeled to express the herpes simplex virus 1 thymidine kinase (*HSV1-tk*) reporter gene. Using this approach, HSV1-tk^{+} CTLs have been efficiently detected in small animals after the infusion of [^{131}I]FIAU or [^{124}I]FIAU by serial images obtained by scintigraphy or PET, respectively.[12,13] Recently, Yaghoubi and colleagues reported the results of studies involving only a single patient with grade IV glioblastoma multiforme (a case report) and demonstrated that ^{18}F-FHBG PET can detect HSV1-tk^{+} T lymphocytes infused intracranially into the site of tumor resection.[14]

In this article, we report the results of repetitive ^{18}F-FEAU PET-CT imaging in two nonhuman primates, which demonstrated that activated autologous T lymphocytes transduced with a retroviral vector encoding for *sr39HSV1-tk* can be detected after intravenous infusion in discrete lymphoid organs and in the sites of inflammation. The results of this preclinical study in nonhuman primates support the application of this technology to noninvasive repetitive imaging of spatial-temporal dynamics of biodistribution of intravenously administered adoptively transferred CTLs in human patients.

Materials and Methods

Retroviral Construct

A retroviral construct was generated encoding for mutant *sr39HSV1-tk* and a truncated form of low-affinity nerve growth factor receptor (LNGFR). Retroviral supernatant was obtained from a stable PG13 retroviral packaging cell line.[15]

Activation, Transduction, and Expansion of Macaque T Lymphocytes

Peripheral blood was obtained from each of the two rhesus macaques (30 mL per animal, obtained in two blood draws) according to Institutional Animal Care and Use Committee (IACUC)-approved procedures. The peripheral blood mononuclear cells (PBMCs) were isolated and cryopreserved. The cells were then thawed, activated, and transduced as previously described.[6,16,17] Seven days after transduction, the NGFR^{+} cells were selected using anti-LNGFR antibody-coated paramagnetic microbeads (Miltenyi, Auburn, CA)[18] and expanded over 20 days, using γ-irradiated human PBMCs, Epstein-Barr virus (EBV) immortalized lymphoblastoid cell lines, and interleukin-2 (100 U/mL)[16] (Proleukin, Chiron, Emeryville, CA) in complete medium (RPMI 1640 [GIBCO-BRL, Carlsbad, CA] 45%, Click’s medium [Irvine Scientific, Santa Ana, CA] 45%, supplemented with 10% fetal bovine serum [FBS] and 2 mmol/L l-glutamine [GIBCO-BRL]). By day 20 of culture, more

than 1×10^9 cells LNGFR$^+$ cells were obtained. Transduction efficiency of the T cells was evaluated by immunophenotyping for LNGFR expression. Cells were stained with PE-conjugated anti-LNGFR and CD3-allophycocyanin (APC) or CD4- and CD8-APC monoclonal antibodies (all from Becton-Dickinson, Mountain View, CA). Cells were analyzed by a FACScan (Becton Dickinson) equipped with the set of filters for triple-label fluorescence quantification and sorting.

In Vitro Radiotracer Uptake Study

An aliquot of sr39HSV1-tk$^+$ T cells was used to measure the uptake of the radiotracer in vitro as previously described.[12] Briefly, untransduced (control) and *sr39HSV1-tk* gene–transduced T cells (3×10^6) were centrifuged at 500 rpm for 2 minutes, resuspended in 1.5 mL of RPMI medium containing 10% FBS plus ^{3}H-FEAU (0.1 μCi/mL) (Moravek, Brea, CA), and incubated for 120 minutes at 37°C in 10 cm^2 dishes. The cells were then transferred to 1.5 mL tubes and centrifuged at 500 rpm for 2 minutes. Supernatant aliquots (100 μL) were transferred to preweighed scintillation vials, the rest of the supernatant was removed by aspiration, and the cell pellet was snap-frozen on dry ice. The frozen pellets were transferred into the preweighed scintillation vials, weighed, and thoroughly disaggregated by vortexing in 0.5 mL of Soluene-350 (Perkin-Elmer, Boston, MA) until fully dissolved and clear. Thereafter, 4 mL of Insta-Fluor Plus scintillation reagent (Perkin-Elmer, Shelton, CT) was added to each vial, and radioactivity concentrations in samples were measured using a Packard Tri-Carb 3100TR scintillation counter (Perkin-Elmer, Shelton, CT). Radioactivity concentration ratios in cell pellet versus medium (dpm/g cells)/(dpm/g medium) were determined (C/M ratio). Each assay was performed in triplicate. The C/M ratio values were plotted versus time of radiotracer accumulation, and a linear regression fit was performed to calculate the rate of the radiotracer accumulation in cells over time (*Ki*, mL/g/min, or min^{-1}). The rate of the radiotracer accumulation in cells reflects the level of *sr39HSV1-tk* gene expression.

Animal Anesthesia and sr39HSV1-tk$^+$ T-Cell Administration

Two healthy adult rhesus macaques (one male and one female with body weights of 13 kg and 8.2 kg, respectively) were used in this study. The macaques were housed separately in an Association for Assessment and Accrediation of Laboratory Animal Care International (AAALAC)-accredited facility. The experiment was performed following M.D. Anderson Cancer Center guidelines for conducting nonhuman primate experiments and under an approved protocol (IACUC protocol #06-07-07281). Prior to the T-cell infusions and imaging, the macaques were premedicated with atropine sulfate and anesthetized with ketamine (10 mg/kg), both administered intramuscularly in the left psoas muscle region, and then intubated endotracheally. General inhalation anesthesia was maintained using 2% isoflurane in oxygen. Electrocardiography, pulse oxymetry, respiration rate, blood pressure, and body temperature were monitored throughout the duration of each imaging session.

Thirty minutes before administration, the sr39HSV1-tk$^+$ T cells were collected by centrifugation at 500 rpm, washed twice with phosphate-buffered solution, resuspended in a normal saline solution, and infused intravenously over 10 to 15 minutes via the left cubital vein.

^{18}F-FEAU PET Imaging

The ^{18}F-FEAU was synthesized using methods described by us previously[13,19] and administered intravenously at a dose of 10.9 MBq/kg (4 mCi/animal) via the right saphenous vein. PET or PET-CT scans were performed at 60 minutes after the tracer injection. For the first macaque, the baseline PET imaging was performed 2 years prior to T-cell infusion on the ECAT Exact HR+ PET scanner (CTI/Siemens, Knoxville, TN). Repeat PET-CT imaging

studies were performed at 90 minutes and 1 week after T-cell infusion on a GE Discovery ST-8 PET-CT scanner (General Electrical Medical System, Milwaukee, WI). For the second macaque, all of the PET-CT studies were performed on the GE Discovery ST-8 PET/CT scanner at baseline (1 week before T-cell infusion) and 90 minutes, 1 day, and 7 days after the intravenous T-cell infusion. During each imaging session, a conventional, noncontracted CT scan was acquired from the head to the toe. Then the whole-body PET scan (from the head to midthighs) was started at 60 minutes after the ^{18}F-FEAU injection. PET images were acquired in two-dimensional mode for 3 minutes per bed position, with four bed positions in total. PET images were reconstructed using *VUE Point* reconstruction software (GE Healthcare), which uses ordered subset expectation maximization (OSEM) algorithm. Emission data were corrected for attenuation and scatter (using CT), random events, and dead-time losses using manufacturer's software.

The CT and PET data were transferred to a dedicated imaging analysis workstation (Hermes Browser, Version 3.0, Hermes Medical Solutions, Stockholm, Sweden). Images were cross-normalized using *Volume Display Program*, Version 1.2 (Hermes Medical Solutions) to accurately compare images obtained on different days of this study. Circular regions of interest (ROI) were placed in the areas with the highest radioactivity as well as in the muscle tissue with a low level of activity. Maximal standardized uptake value (SUV) was calculated from each ROI using the formula SUV = measured activity concentration (Bq/g) × body weight (g)/injected activity (Bq), and the target-to-muscle SUV ratios (T/M ratios) were calculated. For the assessment of radioactivity accumulation in the lungs, the lung area in each transaxial plane on PET images was outlined manually based on corresponding CT images, and the mean SUVs for each slice and for the whole lungs were calculated (a total of 43 planes). Lung to muscle ratios were calculated as well.

PCR for *sr39HSV1-tk* Transgene Expression in Biopsy Samples

Peripheral blood samples were collected at different time points after T-cell infusion. Based on the PET-CT images, an ultrasound-guided core biopsy was obtained from the posterior neck region of the second animal, corresponding to the site of increased ^{18}F-FEAU accumulation at 7 days after T-cell infusion. DNA was extracted from PBMCs and from the needle biopsy using the Qiagen DNA extraction Kit (Qiagen, Valencia, CA). To detect the *sr39HSV1-tk* transgene, 200 ng of DNA was amplified using PCR according to a standard procedure (35 cycles of amplification were used). The sequences of primers used for PCR amplification were HSV1-tk forward primer 5′-CCATAGCAACCGACGTACG-3′ and HSV1-tk reverse primer 5′-GAATCGCGGCCAGCATA-3′.[20] To verify the identity of the *sr39HSV-tk* PCR fragment amplified from the needle biopsy, the PCR product was subcloned into the Topo-TA vector (Invitrogen, Carlsbad, CA) and sequenced by DNA sequencing (CHRC Core Lab, Houston, TX).

Results and Discussion

Autologous sr39HSV1-tk$^+$ T lymphocytes were generated and infused into the rhesus macaques. Animal 1 (male) received 0.8×10^9 cells in 20 mL of saline solution, which were 90% viable and 81% LNGFR$^+$. As shown in Figure 1A and B, for macaque 1, these cells expressed high levels of LNGFR and showed a significant in vitro uptake of the radiotracer ^{3}H-FEAU (40.6 ± 5.3) compared with control cells (1.7 ± 0.11). ^{18}F-FEAU PET images at baseline and 90 minutes and 7 days after sr39HSV1-tk$^+$ T-cell infusion are presented in Figure 1, C to N. Prior to adoptive immunotherapy, the ^{18}F-FEAU-derived radioactivity on PET imaging was predominantly located in the liver, small intestine, kidneys, and urinary bladder, which is consistent with the normal routes of ^{18}F-FEAU excretion through the hepatobiliary and renal systems (see Figure 1C). Ninety minutes after sr39HSV1-tk$^+$ T-cell infusion, PET imaging demonstrated intensive accumulation of ^{18}F-

FEAU-derived radioactivity in the areas of the left parotid gland and in the cervical lymph nodes (see Figure 1D). PET images obtained 7 days after sr39HSV1-tk$^+$ T-cell infusion revealed higher levels of tracer accumulation in the areas of the right parotid gland and right supraclavicular lymph node (see Figure 1E and Table 1). This shift in radiotracer accumulation can be explained, at least in part, by the presence of a mild inflammatory process in the oropharynx of this animal. At 90 minutes after sr39HSV1-tk$^+$ T-cell infusion, a significantly higher accumulation of ^{18}F-FEAU-derived radioactivity was observed in the left psoas muscle and left obturator externus muscle, particularly proximal to the femur, which disappeared from the images obtained 1 week later (see Figure 1M). The location of increased accumulation of ^{18}F-FEAU in that area was at the site of the intramuscular anesthetic injections. It is conceivable that 3.5 hours later, the sr39HSV1-tk-expressing T cells injected into this animal accumulated in that site of inflammation. This explanation seems plausible because 7 days later, no radioactivity was detectable in that area (Figure 1N), whereas a higher accumulation of ^{18}F-FEAU-derived radioactivity was still present in the right posterior supraclavicular lymph node and right parotid gland (Figure 1E). Given that biopsy was not available for this animal, we can only speculate that the trauma-related inflammation was responsible for this observation.

In animal (Figure 2) (female), the baseline ^{18}F-FEAU PET-CT images, obtained 1 week prior to sr39HSV1-tk$^+$ T-cell infusion, demonstrated similar biodistribution of the radiotracer as observed in animal 1 despite the images being obtained with a different scanner (Figure 2C and G). The sr39HSV1-tk$^+$ T-cell product infused in this second animal was similar to that infused in the first animal (0.5×10^9 cells, 90% viable, 81% LNGFR$^+$) with significant in vitro uptake of the radiotracer (Figure 2A and B). At 90 minutes after sr39HSV1-tk$^+$ T-cell infusion, significant accumulation of ^{18}F-FEAU was observed bilaterally, in the posterior cervical regions, which correspond with bilateral posterior cervical lymph nodes (SUV = 2.54 and 1.97 with T/M ratios of 4.21 and 3.25) (see Figure 2D and H). One day after sr39HSV1-tk$^+$ T-cell infusion, the level of ^{18}F-FEAU accumulation in these lymph nodes had significantly decreased (SUV = 1.64 and 1.47 with T/M ratio = 2.33 and 1.77) (Figure 2E and I). However, 1 week later, the level of ^{18}F-FEAU activity somewhat increased (SUV = 1.83 and 2.06 with T/M ratios of 2.26 and 2.56). In addition, a substantial level of ^{18}F-FEAU accumulation was also observed bilaterally in the areas of anterior cervical and axillary lymph nodes (Table 2 and Figure 2F and J). These results were similar to those observed in the first animal (see Table 1 and Figure 1), suggesting that the accumulation of ^{18}F-FEAU radiotracer in the areas of cervical lymph nodes seems a reproducible pattern in these animals and could be due to a preferential localization of polyclonal sr39HSV1-tk$^+$ T cells in areas of chronic inflammatory processes in the oronasopharyngeal region, which are common in these animals. Interestingly, the thymus also showed significant ^{18}F-FEAU accumulation on days 1 and 7. In this second macaque, peripheral blood samples were obtained 4 and 7 days after sr39HSV1-tk$^+$ T-cell infusion. We found that circulating sr39HSV1-tk$^+$ T cells expressing LNGFR were detectable in blood by FACS analysis (Figure 3A). Moreover, we also obtained a needle biopsy of a cervical lymph node in which a significant uptake of the radiotracer was observed at 7 days after sr39HSV1-tk$^+$ T-cell infusion. In this sample, we confirmed the presence of the *sr39HSV1-tk* transgene by deoxyribonucleic acid (DNA) PCR amplification (Figure 3B) indicating that the specific accumulation of the radiotracer was due to the presence of sr39HSV1-tk$^+$ T cells.

It is noteworthy that in the current study, we did not observe significant accumulation of sr39HSV1-tk$^+$ T cells in the lung as frequently observed in imaging experiments conducted in small animals.[12] However, in animal 1, by quantitative analysis, we determined that the whole-lung radioactivity was 38.5% higher on the PET images obtained at 90 minutes following T-cell infusion compared with images obtained 1 week later, suggesting only a

transient diffuse retention of T cells in lungs (see Table 1). The current study is substantially different from that of Yaghoubi and colleagues, for which a single imaging time point after direct injection of autologous human tk^+ T cells into the resected cranial tumor was reported.[14] Our study is the first to demonstrate the feasibility of repetitive PET-CT imaging of spatial-temporal dynamics of distribution and trafficking of *sr39HSV1-tk* reporter gene–expressing T cells in non human primates after intravenous administration.

We conclude that PET imaging with ^{18}F-FEAU may be used in future clinical trials to evaluate the biodistribution of adoptively transferred CTLs modified to express the *sr39HSV1-tk* reporter gene or its variants.[21] This technology will ultimately allow for long-term monitoring of trafficking patterns and persistence of the T cells in patients and facilitate critical improvements in T-cell therapy for cancer.

Acknowledgments

We thank Dana Toomey, Julie Basham, Deborah Petit, Alfredo Santiago, and Jennifer Miller for their excellent technical support and Nancy Swanston for excellent coordination of this study. Financial disclosure of authors: This work was supported by the Dana Foundation Award “Clinical Concepts in Neuro-Immuno Imaging” (to J.G.), the New Research Program Development Fund of the Department of Experimental Diagnostic Imaging (to J.G. and M.A.), The University of Texas M.D. Anderson Cancer Center, and a Baylor College of Medicine-M.D. Anderson Multi-Institutional Research Grant (to G.D., C.M.B., E.J.S.).

References

1. Dudley ME, Yang JC, Sherry R, et al. Adoptive cell therapy for patients with metastatic melanoma: evaluation of intensive myeloablative chemoradiation preparative regimens. J Clin Oncol. 2008; 26:5233–5239. [PubMed: 18809613]
2. Yee C, Thompson JA, Byrd D, et al. Adoptive T cell therapy using antigen-specific CD8+ T cell clones for the treatment of patients with metastatic melanoma: in vivo persistence, migration, and antitumor effect of transferred T cells. Proc Natl Acad Sci U S A. 2002; 99:16168–16173. [PubMed: 12427970]
3. Bollard CM, Aguilar L, Straathof KC, et al. Cytotoxic T lymphocyte therapy for Epstein-Barr virus+ Hodgkin’s disease. J Exp Med. 2004; 200:1623–1633. [PubMed: 15611290]
4. Straathof KC, Bollard CM, Popat U, et al. Treatment of nasopharyngeal carcinoma with Epstein-Barr virus–specific T lymphocytes. Blood. 2005; 105:1898–1904. [PubMed: 15542583]
5. Comoli P, Pedrazzoli P, Maccario R, et al. Cell therapy of stage IV nasopharyngeal carcinoma with autologous Epstein-Barr virus-targeted cytotoxic T lymphocytes. J Clin Oncol. 2005; 23:8942–8949. [PubMed: 16204009]
6. Pule MA, Savoldo B, Myers GD, et al. Virus-specific T cells engineered to coexpress tumor-specific receptors: persistence and antitumor activity in individuals with neuroblastoma. Nat Med. 2008; 14:1264–1270. [PubMed: 18978797]
7. Morgan RA, Dudley ME, Wunderlich JR, et al. Cancer regression in patients after transfer of genetically engineered lymphocytes. Science. 2006; 314:126–129. [PubMed: 16946036]
8. Heslop HE, Ng CY, Li C, et al. Long-term restoration of immunity against Epstein-Barr virus infection by adoptive transfer of gene-modified virus-specific T lymphocytes. Nat Med. 1996; 2:551–555. [PubMed: 8616714]
9. Rosenberg SA, Aebersold P, Cornetta K, et al. Gene transfer into humans—immunotherapy of patients with advanced melanoma, using tumor-infiltrating lymphocytes modified by retroviral gene transduction. N Engl J Med. 1990; 323:570–578. [PubMed: 2381442]
10. Till BG, Jensen MC, Wang J, et al. Adoptive immunotherapy for indolent non-Hodgkin lymphoma and mantle cell lymphoma using genetically modified autologous CD20-specific T cells. Blood. 2008; 112:2261–2271. [PubMed: 18509084]
11. Savoldo B, Goss JA, Hammer MM, et al. Treatment of solid organ transplant recipients with autologous Epstein Barr virus-specific cytotoxic T lymphocytes (CTLs). Blood. 2006; 108:2942–2949. [PubMed: 16835376]

12. Koehne G, Doubrovin M, Doubrovina E, et al. Serial in vivo imaging of the targeted migration of human HSV-TK-transduced antigen-specific lymphocytes. Nat Biotechnol. 2003; 21:405–413. [PubMed: 12652311]

13. Soghomonyan S, Hajitou A, Rangel R, et al. Molecular PET imaging of HSV1-tk reporter gene expression using [^{18}F] FEAU. Nat Protoc. 2007; 2:416–423. [PubMed: 17406603]

14. Yaghoubi SS, Jensen MC, Satyamurthy N, et al. Noninvasive detection of therapeutic cytolytic T cells with ^{18}F-FHBG PET in a patient with glioma. Nat Clin Pract Oncol. 2009; 6:53–58. [PubMed: 19015650]

15. Kornblau SM, Aycox PG, Stephens C, et al. Control of graft-versus-host disease with maintenance of the graft-versus-leukemia effect in a murine allogeneic transplant model using retrovirally transduced murine suicidal lymphocytes. Exp Hematol. 2007; 35:842–853. [PubMed: 17577932]

16. Berger C, Jensen MC, Lansdorp PM, et al. Adoptive transfer of effector CD8^{+} T cells derived from central memory cells establishes persistent T cell memory in primates. J Clin Invest. 2008; 118:294–305. [PubMed: 18060041]

17. Vera J, Savoldo B, Vigouroux S, et al. T lymphocytes redirected against the kappa light chain of human immunoglobulin efficiently kill mature B lymphocyte-derived malignant cells. Blood. 2006; 108:3890–3897. [PubMed: 16926291]

18. Bonini C, Grez M, Traversari C, et al. Safety of retroviral gene marking with a truncated NGF receptor. Nat Med. 2003; 9:367–369. [PubMed: 12669036]

19. Alauddin MM, Shahinian A, Park R, et al. In vivo evaluation of 2′-deoxy-2′-[^{18}F]fl uoro-5-iodo-1-beta-D-arabinofuranosyluracil ([^{18}F]FIAU) and 2′-deoxy-2′-[^{18}F]fl uoro-5-ethyl-1-beta-D-arabinofuranosyluracil ([^{18}F]FEAU) as markers for suicide gene expression. Eur J Nucl Med Mol Imaging. 2007; 34:822–829. [PubMed: 17206416]

20. Traversari C, Marktel S, Magnani Z, et al. The potential immunogenicity of the TK suicide gene does not prevent full clinical benefit associated with the use of TK-transduced donor lymphocytes in HSCT for hematologic malignancies. Blood. 2007; 109:4708–4715. [PubMed: 17327417]

21. Najjar AM, Nishii R, Maxwell DS, et al. Molecular-genetic PET imaging using an HSV1-tk mutant reporter gene with enhanced specificity to acycloguanosine nucleoside analogs. J Nucl Med. 2009; 50:409–416. [PubMed: 19223410]

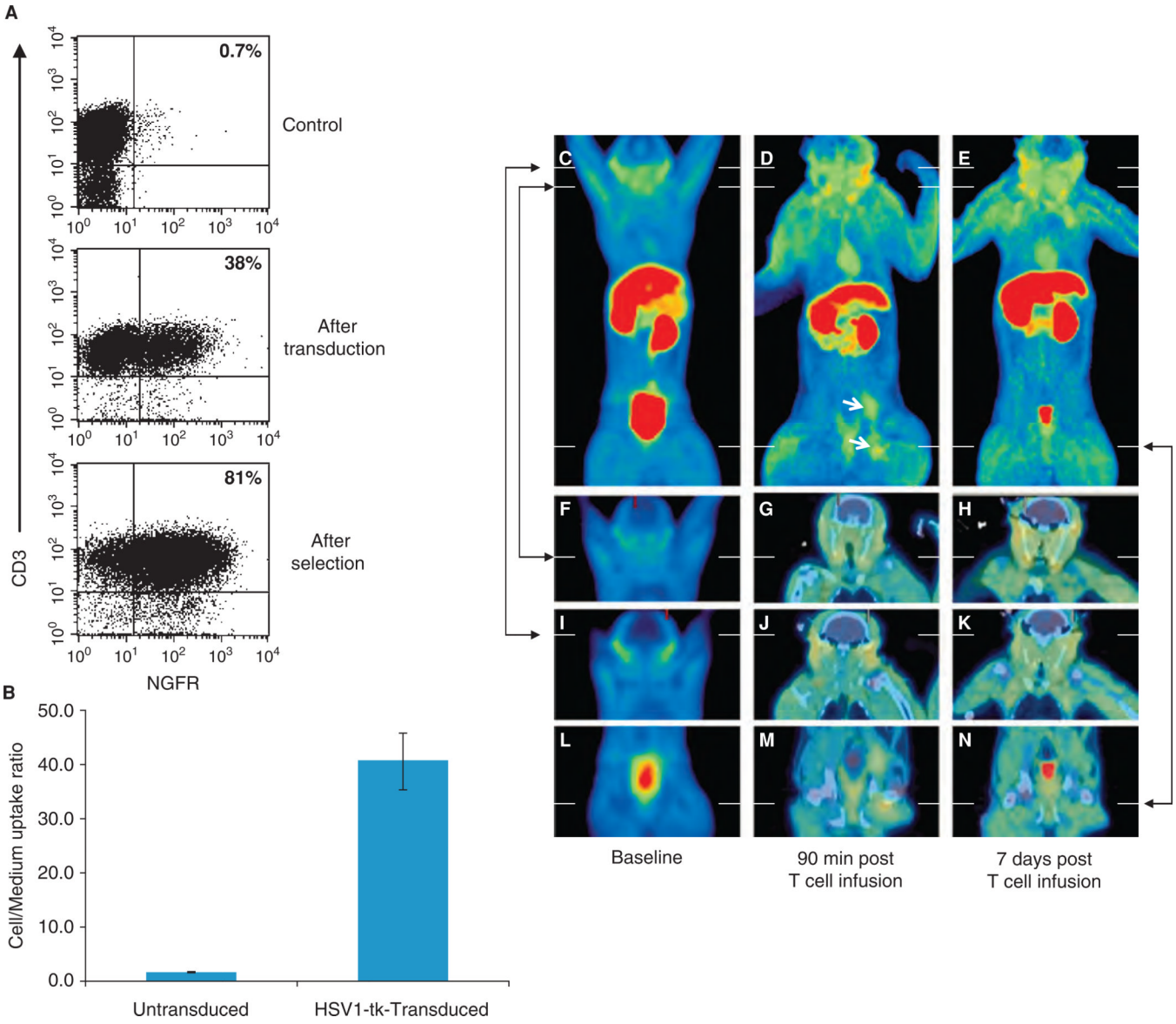

Figure 1.

Repetitive PET-CT images of ^{18}F-FEAU distribution in the rhesus macaque 1 before and after injection of sr39HSV1-tk$^+$ autologous T lymphocytes. *A* illustrates the percentage of LNGFR$^+$ T lymphocytes, as assessed by FACS analysis using a monoclonal antibody detecting NGFR (Becton-Dickinson), 7 days after retroviral transduction and at the time of infusion after selection using LNGFR microbeads. *B* illustrates the uptake of [^{3}H]-FEAU by sr39HSV1-tk$^+$ T lymphocytes. Each assay was performed in triplicate. Sr39HSV1-tk$^+$ T cells exhibited a cell to medium uptake ratio of 40.6, 24.5× higher than the control. *Columns* represent means; *bars* indicate ± standard deviation. *C* to *N* illustrate the whole-body PET scan 60 minutes after the tracer injection. PET images were reconstructed, analyzed, and normalized as previously described.[12] *C*, *D*, and *E* represent maximum-intensity three-dimensional projections of whole-body PET images collected before T-cell infusion (*C*) and 90 minutes (*D*) and 7 days (*E*) after T-cell infusion. *F*, *G*, *H*, *I*, *J*, and *K* demonstrate the differences in ^{18}F-FEAU accumulation in the parotid glands and cervical lymph nodes between baseline (*F*, *I*), 90 minutes (*G*, *J*), and 7 days (*H*, *K*) after T-cell administration. *L*,

M, and *N* represent coronal PET or PET-CT images through the area of target lesions in the left thigh visible at 90 minutes after T-cell administration and 60 minutes after ^{18}F-FEAU injection (*M*), which is absent in the baseline image (*L*) and 7 days later (*N*).

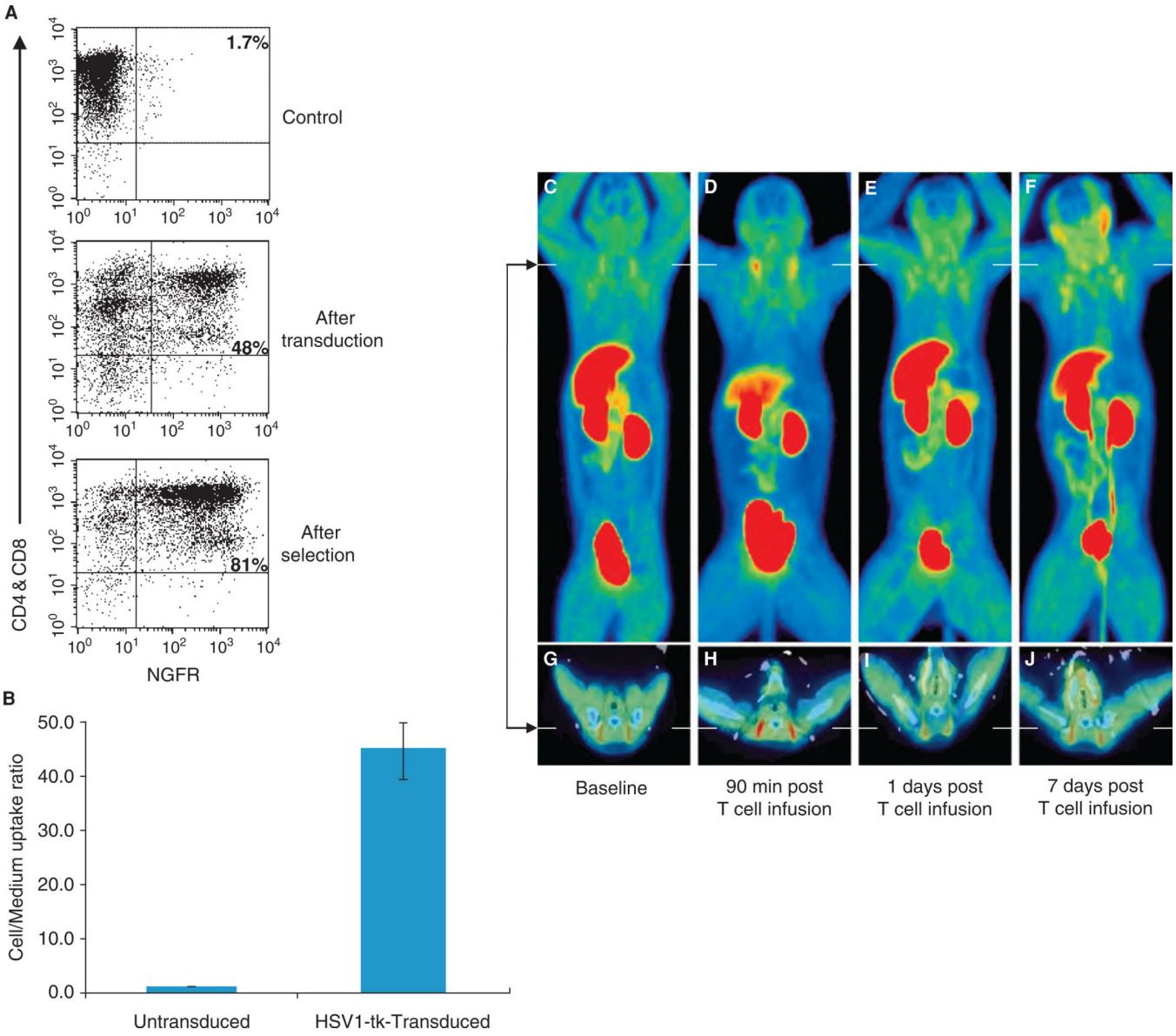

Figure 2.

Repetitive PET-CT images of ^{18}F-FEAU distribution in the rhesus macaque 2 before and after injection of sr39HSV1-tk^{+} autologous T lymphocytes. *A* illustrates the characteristics of the T-cell product as described in Figure 1. *B* illustrates the uptake of [^{3}H]-FEAU by sr39HSV1-tk^{+} T lymphocytes. Sr39HSV1-tk^{+} T cells exhibited a cell to medium uptake ratio of 45.2, 32.2 × higher than the control. *Columns* represent means; *bars* indicate ± standard deviation. *C* to *F* represent maximum-intensity three-dimensional projections of whole-body PET images obtained at baseline (*C*) and 90 minutes (*D*), 1 day (*E*), and 7 days (*F*) after T-cell infusion. *G* to *J* represent transaxial PET-CT images through the area of posterior cervical lymph nodes at each time point.

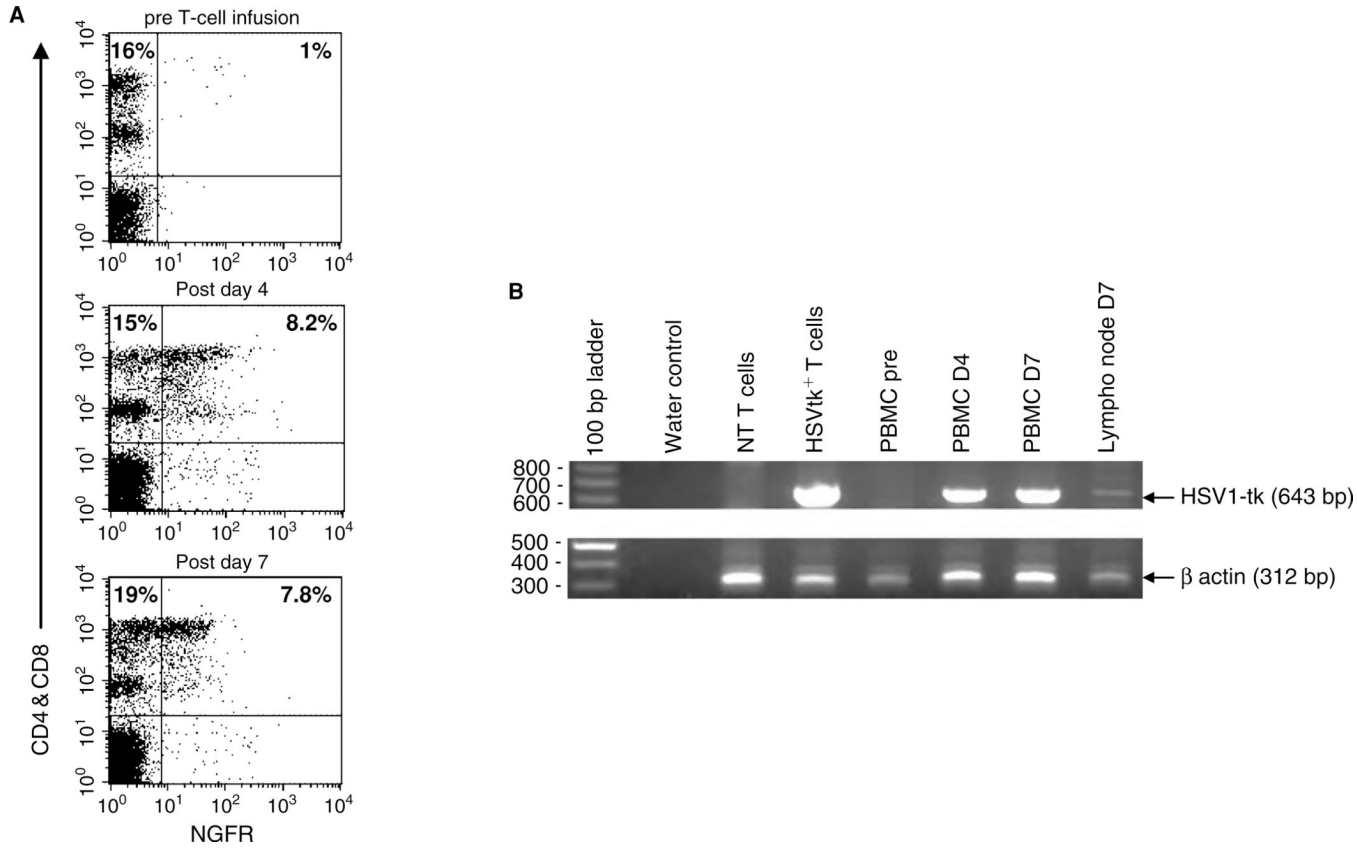

Figure 3.

Detection of sr39HSV1-tk$^+$ T lymphocytes in peripheral blood and in a posterior neck lymph node biopsy. *A* illustrates the detection of circulating NGFR$^+$ T cells as assessed by phenotypic analysis in blood samples collected before and after T-cell infusion. *B* illustrates the detection of sr39HSV-tk$^+$ expression by polymerase chain reaction in peripheral blood mononuclear cells (PBMCs) preinfusion, 4 days postinfusion, and 7 days postinfusion and in a posterior neck lymph node biopsy sample obtained 7 days after T-cell infusion. Ex vivo expanded T nontransduced cells and ex vivo expanded sr39HSV1-tk$^+$ T cells were also used as negative and positive control, respectively.

Table 1

Quantification of ^{18}F-FEAU Radioactivity in Target Sites and Muscles (Reference Tissues) in Monkey 1

Location	Baseline		90 min Post T-Cell Injection		7 d Post T-Cell Injection	
	SUV*	T/M Ratio	SUV*	T/M Ratio	SUV*	T/M Ratio
Right parotid gland	0.75	1.80	2.12	1.72	2.22	2.25
Left parotid gland	0.74	2.08	3.02	2.56	1.91	1.73
Right submandibular lymph node	0.74	1.66	2.52	2.04	2.14	1.71
Left submandibular lymph node	0.71	1.59	2.66	2.02	1.84	1.51
Right posterior cervical lymph node	0.66	1.02	1.73	1.56	2.55	2.25
Left posterior cervical lymph node	0.69	1.06	1.71	1.45	2.32	1.96
Right axillary lymph node	0.59	1.04	1.52	1.34	1.87	1.63
Left axillary lymph node	0.58	1.02	1.44	1.19	2.09	1.68
Thymus	0.59	1.01	1.37	1.05	1.60	1.26
Left psoas muscle	0.65	1.21	2.32	1.98	1.14	0.94
Left obturator externus muscle	0.55	1.03	2.88	2.63	1.36	0.98
Lung†	0.23	0.45	0.65	0.60	0.48	0.43

SUV = standardized uptake value; T/M ratio = target to muscle ratio.

*Maximum SUV.

†Mean SUV.

Table 2

Quantification of ^{18}F-FEAU Radioactivity in Target Sites and Muscles (Reference Tissues) in Monkey 2

Location	Baseline		90 min Post T-Cell Injection		1 d Post T-Cell Injection		7 d Post T-Cell Injection	
	SUV*	T/M Ratio	SUV*	T/M Ratio	SUV*	T/M Ratio	SUV*	T/M Ratio
Right parotid gland	1.12	1.51	1.04	1.81	1.36	1.80	2.13	2.08
Left parotid gland	1.15	1.56	1.04	1.81	1.30	1.72	2.75	2.61
Right submandibular lymph node	1.05	1.48	0.80	1.27	1.53	2.25	1.62	1.96
Left submandibular lymph node	1.11	1.66	0.70	1.16	1.21	1.69	2.01	2.48
Right posterior cervical lymph node	1.55	2.24	2.54	4.21	1.64	2.33	1.83	2.26
Left posterior cervical lymph node	1.55	2.36	1.97	3.25	1.47	1.77	2.06	2.56
Right axillary lymph node	1.41	1.63	1.01	1.41	1.58	1.95	2.17	2.14
Left axillary lymph node	1.35	1.50	1.00	1.39	1.43	1.81	2.11	2.31
Thymus	1.10	1.17	0.93	1.19	1.49	1.63	1.41	1.42
Lung†	0.24	0.30	0.21	0.32	0.24	0.28	0.23	0.30

SUV = standardized uptake value; T/M ratio = target to muscle ratio.

*Maximum SUV.

†Mean SUV.